NANO LETTERS

Letter

pubs.acs.org/NanoLett

Transient Clustering of Reaction Intermediates during Wet Etching of Silicon Nanostructures

Zainul Aabdin,[†,‡,§,∥] Xiu Mei Xu,[⊥] Soumyo Sen,[#] Utkarsh Anand,[†,‡,§,∥] Petr Král,[#,▽,●] Frank Holsteyns,[⊥] and Utkur Mirsaidov*[,†,‡,§,∥]

[†]Department of Physics, National University of Singapore, 117551, Singapore

[‡]Centre for BioImaging Sciences and Department of Biological Sciences, National University of Singapore, 117557, Singapore

[§]Centre for Advanced 2D Materials and Graphene Research Centre, National University of Singapore, 117546, Singapore

[∥]NUSNNI-NanoCore, National University of Singapore, 117411, Singapore

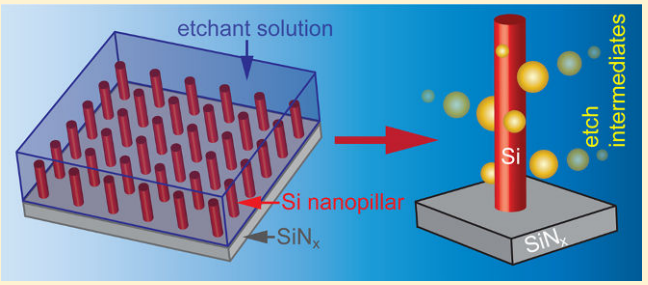
[⊥]imec, Kapeldreef 75, Leuven, B-3001, Belgium

[#]Department of Chemistry, [▽]Department of Physics, University of Illinois at Chicago, Chicago, Illinois 60607, United States

[●]Department of Biopharmaceutical Sciences, University of Illinois at Chicago, Chicago, Illinois 60612, United States

Supporting Information

ABSTRACT: Wet chemical etching is a key process in fabricating silicon (Si) nanostructures. Currently, wet etching of Si is proposed to occur through the reaction of surface Si atoms with etchant molecules, forming etch intermediates that dissolve directly into the bulk etchant solution. Here, using in situ transmission electron microscopy (TEM), we follow the nanoscale wet etch dynamics of amorphous Si (a-Si) nanopillars in real-time and show that intermediates generated during alkaline wet etching first aggregate as nanoclusters on the Si surface and then detach from the surface before dissolving in the etchant solution. Molecular dynamics simulations reveal that the molecules of etch intermediates remain weakly bound to the hydroxylated Si surface during the etching and aggregate into nanoclusters via surface diffusion instead of directly diffusing into the etchant solution. We confirmed this model experimentally by suppressing the formation of nanoclusters of etch intermediates on the Si surfaces by shielding the hydroxylated Si sites with large ions. These results suggest that the interaction of etch intermediates with etching surfaces controls the solubility of reaction intermediates and is an important parameter in fabricating densely packed clean 3D nanostructures for future generation microelectronics.



KEYWORDS: *Nanofabrication, nanopillars, nanowires, silicon, chemical etching, reaction intermediates, in situ transmission electron microscopy (TEM), liquid cell*

The continuing drive for faster and more energy-efficient microelectronic components requires the fabrication of smaller, denser, and better-defined nanostructures. For current-generation devices based on planar 2D layouts, the increase in device density is achieved by reducing their planar sizes. However, with some current features already several tens of atoms wide, following Moore's law has become extremely challenging.[1,2] Therefore, the newest and future generations of devices are based on 3D nanodevice architectures.[3] For example, the latest generation gate-all-around field effect transistors are now incorporating vertical semiconductor nanowires or nanopillars, which serve as channels for charge carriers; the carrier flow is controlled by metal gates that wrap around these vertical channels.[2,4,5] Vertical nanowires are also finding applications in solar cells,[6] lasers,[7] photodetectors,[8] and nanoelectromechanical systems.[9]

However, fabricating 3D semiconductor nanostructures, for example, nanowires, by present methods such as vapor−liquid−solid (VLS) mechanism based growth using catalysts seeded on substrates[10,11] or dry plasma etching of bulk semiconductors[12] poses challenges not faced with simpler 2D designs. As the aspect ratio and density of vertical nanowires increase with each device generation, significant difficulties emerge in producing an ordered array of smaller diameter nanowires using the VLS method,[13] while dry etching methods lead to plasma-induced damage to the semiconductor surface. These surface defects drastically reduce the mobility of charge carriers and thus degrade device performance and reliability.[14] In contrast, chemical wet etching (post VLS growth or dry-etching) can

Received: January 16, 2017
Revised: April 7, 2017
Published: April 18, 2017

ACS Publications © 2017 American Chemical Society

DOI: 10.1021/acs.nanolett.7b00196
Nano Lett. 2017, 17, 2953−2958

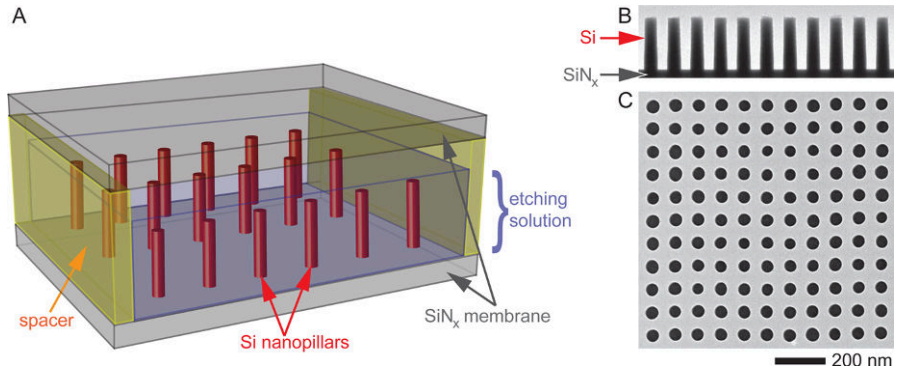


Figure 1. Experimental configuration: amorphous Si (a-Si) nanopillars on SiN_x membrane. (A) Schematic of a liquid cell with a-Si nanopillars used for real-time imaging of wet etching process. A series of 200 nm tall and 45 nm diameter a-Si nanopillars are fabricated on a bottom SiN_x membrane at a density of 1.2×10^{10} cm^{-2}; the two membranes are separated by a 240 nm spacer. The nanopillars are then immersed in an etchant (KOH) solution that fills the liquid cell, and the resulting etching process is observed inside a TEM. TEM images of free-standing a-Si nanopillars on SiN_x membrane showing (B) side and (C) top-down views.

be tuned to produce small diameter nanostructures with damage-free surfaces.[15] Moreover, the high selectivity of wet etching processes for different materials or semiconductor doping levels enables more control over the geometry of nanowires.[16]

Despite the technological importance of chemical wet etching in semiconductor micro- and nanofabrication, our understanding of wet etching dynamics at the nanoscale is inferred from studies in bulk etching conditions. Etching is a complex process that involves the formation of intermediates that are then transformed into soluble molecules. However, it is not clear how these reaction intermediates are removed from the etching surfaces by etchant solutions.[17,18] The accumulation of unwanted byproducts on the etching surfaces during wet or dry etching may lead to increased surface roughness and nonuniformities[19] that can diminish the performance and reliability of fabricated nanodevices.[20,21] Current methods are unable to monitor the wet etching processes in real-time at the nanoscale level.

To understand wet etching dynamics at the nanoscale level, we have taken a direct approach of imaging these intermediate steps by in situ transmission electron microscopy (TEM).[22,23] We can directly watch the thinning of densely packed amorphous Si (a-Si) nanopillars during etching in an aqueous potassium hydroxide (KOH) solution—a widely used etchant in Si microfabrication.[24−26] Contrary to our expectations, our observations reveal that nanoclusters of etch intermediates form and grow on the Si surface during wet etching. These intermediates later detach and dissolve in the etchant solution.

A periodic array of free-standing a-Si nanopillars used in our experiments is fabricated on a SiN_x membrane (Figure 1B−C) and assembled into a liquid cell (Figure 1A) with a top electron-translucent SiN_x window separated by a spacer (SI Sections 1−2). The nanopillars are etched by a KOH solution at room temperature and imaged at a rate of 10 frames per second in the TEM at 200 kV and at a low electron flux of 5−25 e/(Å^2·s), which has a negligible effect on the observed etching dynamics (SI Sections 7−9, 18).

Real-time observations (Figure 2A−B and Figure 3A−C) reveal that, as the diameters of the a-Si nanopillars decrease during wet etching, 2−20 nm nanocluters of etch intermediates continuously form on the nanopillar surfaces, detach from the nanopillars, and dissolve in the solution, leaving no visible residues when etch is completed (Figure 2A, t = 426.7 s, and

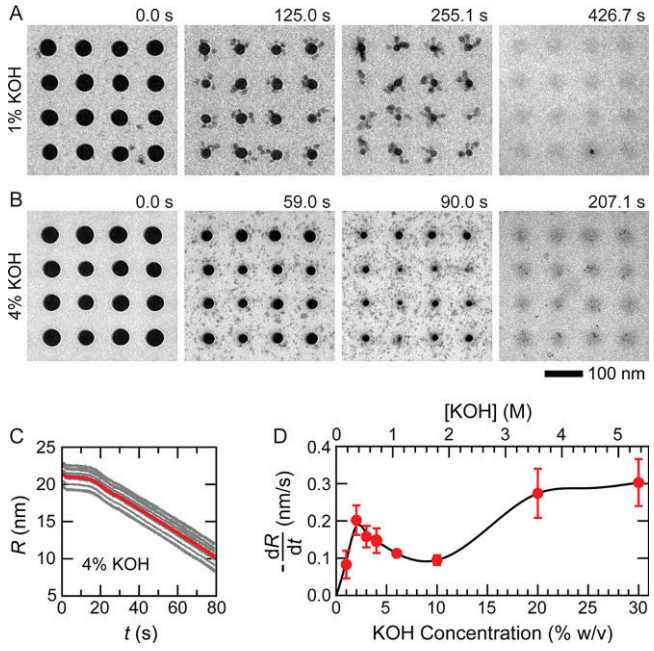


Figure 2. Etch dynamics of a-Si nanopillars in solution with different KOH concentrations. A series of TEM images showing the etching process of a-Si nanopillars in (A) 1% (Supporting Video S1) and (B) 4% (w/v) (Supporting Video S2) aqueous KOH solution. As soon as the etching of a-Si nanopillars begins, nanoclusters of etching intermediates that are 2−20 nm in size begin forming on the nanopillars. At the end of the etching process, when a-Si nanopillars are fully consumed, nanoclusters are fully dissolved in the solution (t = 426.7 s and t = 207.1 s). (C) Radius of nanopillars in 4% KOH solution shown in (B) as a function of time. Gray: radius of 16 individual a-Si nanopillars; Red: average radius of all 16 nanopillars. (D) Average etch rate of a-Si nanopillars, $-dR/dt$, vs KOH concentration. The solid black line is a visual guide.

Figure 2B, t = 207.1 s) (Supporting Videos S1−2). From the change in nanopillar radii at different KOH concentrations (Figure 2C), we calculate the etch rates (Figure 2D), which follows a complex nonmonotonic relationship with a sharp peak of 0.2 nm/s at 2% (w/v) KOH, a minimum of 0.1 nm/s at 5−10% (w/v) KOH, and a broad maximum of 0.3 nm/s at 20−30% (w/v) KOH. Similar plots are obtained for bulk etching of planar crystalline Si surfaces[25,27] (SI Section 11) indicating that

DOI: 10.1021/acs.nanolett.7b00196
Nano Lett. 2017, 17, 2953−2958

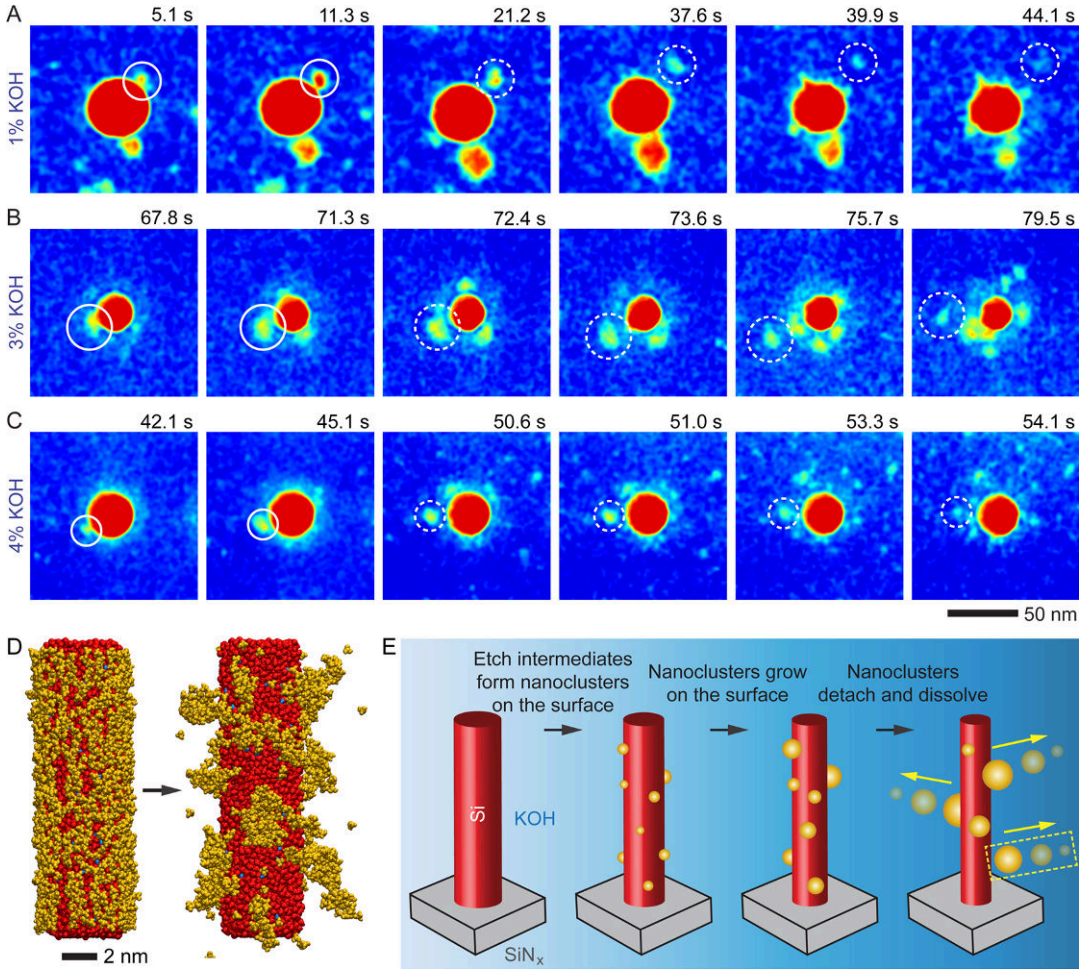


Figure 3. Mechanism of a-Si nanopillar etching by KOH. Time-resolved in situ TEM image series in false color showing formation and growth of the nanoclusters of intermediates (white solid circles), followed by its detachment and dissolution (white dashed circles) in (A) 1%, (B) 3%, and (C) 4% (w/v) KOH solutions. (D) Atomistic MD simulation showing the aggregation of 935 $Si(OH)_4$ molecules (orange) on the surface of a Si nanopillar (length: 17 nm, diameter: 4.5 nm) with H-terminated Si (red) and hydroxyl-terminated Si (blue) atoms. Water molecules and ions are not shown for clarity. Left and right images correspond to $t = 0$ ns and $t = 30$ ns, respectively. (E) Schematic illustration of a two-step etching mechanism: (i) the formation and growth of nanoclusters on the surface of the nanopillars, and (ii) the detachment and subsequent dissolution of the nanoclusters in the etchant solution.

the underlying mechanisms at the nanoscale and bulk scale are similar.

The transient clustering of etch intermediates, not reported previously, can pose a significant problem in fabricating densely packed nanostructures. To understand the spatiotemporal dynamics of these processes, we tracked how the nanoclusters evolved in real-time (Figure 3A–C). During the etching process, individual nanoclusters initially form and grow on the nanopillar surface; they then detach and move into the etchant solution. Once in the solution, these nanoclusters slowly dissolve (Figure 3A–C, E). We have observed this process for all tested ranges of KOH concentrations (1–30% w/v) (SI Section 13). Our results clearly show that the initial aggregation of reaction intermediates into nanoclusters occurs on the surface prior to their detachment and not in the etchant solution.

Previous studies of the wet etching mechanism have proposed that alkaline solutions such as KOH erode a Si surface through sequential chemical reactions[24,25,28] (SI Section 11). In the first rate-limiting step, hydrogen-terminated Si atoms on the surface oxidize to form hydroxyl-terminated (hydroxylated) Si atoms ($=Si^{-H}_{-H} \rightarrow =Si^{-OH}_{-OH}$).[29] The hydroxylation of surface Si atoms has two effects: (i) it weakens their Si–Si back bonds because of the stronger electronegativity of O compared to Si, and (ii) it exposes these Si–Si back bonds to attack by water molecules.[30] For each broken Si–Si bond, the H and OH of an involved water molecule terminate the inner Si atom and hydroxyl-terminated surface Si atom, respectively.[30] Consequently, the surface Si atom is removed as a monosilicic acid ($Si(OH)_4$), a poorly soluble intermediate etching product, leaving behind another hydrogen-terminated Si surface.[28] Later, the $Si(OH)_4$ intermediate molecule is converted into a soluble silicate anion, $SiO_2(OH)_2^{2-}$, which readily dissolves in the alkaline solution.[24] The $Si(OH)_4$ intermediates are thought to diffuse directly from the Si surface without forming a transient nanoclusters. It is also important to note that during wet etching of a-Si nanopillars, H_2 gas is produced as a reaction byproduct[24,27] (SI Section 11). In bulk water at a pressure of 1 atm, the saturation concentration of H_2 gas is very low ($c_{sat(H_2)} \approx 0.8$ mM),[31] and the nucleation of H_2 nanobubbles is generally expected. However, in our experiments we did not detect nanobubbles. This is most likely due to a very slow production rate of H_2,

DOI: 10.1021/acs.nanolett.7b00196
Nano Lett. 2017, 17, 2953–2958

owing to slow Si etch rates at room temperature, and fast upward diffusion of H_2 into air gaps in the loading pockets of our liquid cells (Figure 1 and Figure S1).

Given this multistep dynamics of Si wet etching, it is important to clarify the nature of the nanoclusters formed on Si surfaces during their etching. We hypothesize that the intermediate molecules ($Si(OH)_4$) cluster on the Si surface before being converted into soluble silicate anions ($SiO_2(OH)_2^{2-}$). To check this hypothesis, we modeled the dynamics of $Si(OH)_4$ intermediates on wet etched Si surface by atomistic molecular dynamics (MD) simulations. Initially, $Si(OH)_4$ molecules were uniformly distributed on the hydrogen- and hydroxyl-terminated surface of the Si nanopillar (Figure 3D) (SI Section 17). The simulations show that $Si(OH)_4$ intermediate products reorganize on the nanopillar surface into small nanoclusters instead of moving into solution (Figure 3D). The neighboring nanoclusters further aggregate into larger surface-bound clusters that closely resemble the nanoclusters that we imaged in our in situ TEM experiments (Figure 3A–C). The $Si(OH)_4$ clusters are held on the Si nanopillar surface, with less than ~3% of the $Si(OH)_4$ intermediates escaping into the solution during the simulation.

The model confirms that the hydroxylated Si surface weakly attracts the intermediate $Si(OH)_4$ molecules and their clusters. The aggregation of $Si(OH)_4$ intermediates into nanoclusters is consistent with the strong hydrogen bonding between these intermediates[32,33] (SI Section 17, Figure S20). Small amounts of other silicate species that form as a result of the oligomerization of silicic acid molecules can also participate as intermediate products[34,35] (SI Section 12) and be potentially present within the experimentally observed intermediate nanoclusters. Nevertheless, throughout the entire etching process and regardless of the composition of the nanoclusters, these etching intermediates are transported from the surface into the etchant solution in the form of nanoclusters, where they dissolve.

Our simulations also reveal that, in the absence of the hydroxide groups on the surface of Si nanopillars, the $Si(OH)_4$ intermediates do not remain on the nanopillar surface but directly diffuse into the solution (SI Section 17, Figure S19). Therefore, blocking the interactions between hydroxyl-terminated surface Si atoms and the $Si(OH)_4$ intermediates should inhibit their cluster formation. We tested this prediction with two complementary approaches. First, because TMA^+ cations of tetramethylammonium hydroxide (TMAH) are known to screen hydroxylated surface Si atoms,[36] we reasoned that these large counterions will sterically shield the hydroxylated sites. In this follow up experiments, we observed no nanoclusters of intermediates forming on the surfaces as the nanopillars are etched in TMAH etching solution (Figure 4A, Supporting Video S3) or even when KOH is added to TMAH etching solution (Figure 4B, Supporting Video S4) (SI Section 14). This observation is consistent with our simulations showing that hydroxyl groups on the Si surface are primarily responsible for holding the nanoclusters of the intermediates at the nanopillar surface. Because TMA^+ ions physically block access to hydroxylated sites, the intermediates must move directly into the solution without clustering on the surface. This shielding by counterions, which also limits the access of etchant, is consistent with slightly slower etch rates of Si in TMAH solutions[26] (Figure S15).

A complementary approach for blocking the access to surface hydroxyl groups during etching can be achieved through

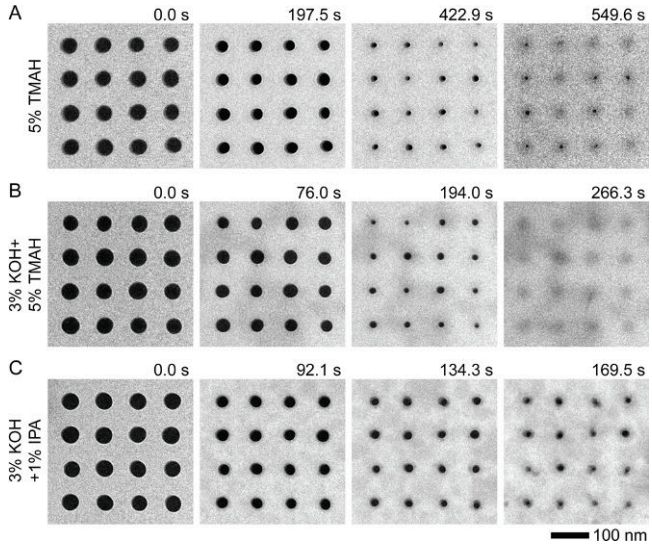


Figure 4. Etching dynamics of a-Si nanopillars in the presence of TMAH and alcohol. A series of TEM images showing the etching dynamics of a-Si nanopillars by (A) 5% (w/v) (550 mM) TMAH (Supporting Video S3), (B) 3% (w/v) KOH and 5% (w/v) TMAH (Supporting Video S4), and (C) 3% (w/v) KOH and 1% (v/v) isopropyl alcohol (Supporting Video S5) solutions. No formation of nanoclusters of intermediates is observed during these etching processes.

termination of Si atoms with alcohols. An alcohol (HOR) in an alkaline aqueous solution partially dissociates ($HOR \rightarrow H^+ + OR^-$) to form alkoxide ions (OR^-). These alkoxide groups on the surface should terminate a fraction of the surface Si atoms ($=Si^{-H}_{-H} \rightarrow =Si^{-OR}_{-OH}$), thus sterically screening the Si surface during etching[37,38] and consequently hindering the interaction between hydroxyl-terminated Si atoms and the etching intermediates. When we monitored the nanopillar etching dynamics in an aqueous KOH solution mixed with isopropyl alcohol (Figure 4C, Supporting Video S5), the nanoclusters were not detected on the surface or in the etching solution (Figure 4C) (SI Section 15). These experiments strongly support the model that surface hydroxyls provide anchoring sites for etch intermediates to aggregate and introduce methods to prevent etch byproducts from forming nanoclusters on the Si substrate surface.

Our study provides three important insights into the chemical wet etch fabrication methods. First, our observations show that the wet etching of vertical a-Si nanostructures in KOH occurs in two distinct steps: (i) the formation and growth of intermediate Si products into nanoclusters on the nanostructure surface, followed by (ii) the detachment and dissolution of these clustered intermediates in the etchant solution. Second, the formation of surface-bound nanoclusters of etch intermediates is a transient step through which the intermediates are effectively removed from the surfaces and can be common in other wet etching reactions of amorphous materials. Although transient, the nanoclusters may limit the access of etchants to surfaces and give rise to surface contaminants that arise during conventional KOH etching processes. Third, we can prevent clustering of intermediates on the surface by molecular shielding of hydroxyl-terminated surface Si atoms, sticky sites, which offers a strategy to maintain byproduct-free surfaces during wet etching. We expect the clustering of surface-bound etch-intermediates to be less on

DOI: 10.1021/acs.nanolett.7b00196
Nano Lett. 2017, 17, 2953–2958

smooth surfaces of crystalline Si nanostructures, because the density of OH-terminated sites is higher on rough surfaces of a-Si structures. In general, the ability to observe and control etching processes at the nanoscale and in real-time by in situ TEM will certainly improve the design of new top-down nanofabrication processes for next-generation nanoscale devices.

■ ASSOCIATED CONTENT

Supporting Information

The Supporting Information is available free of charge on the ACS Publications website at DOI: 10.1021/acs.nanolett.7b00196.

Materials and methods, additional experiments, and relevant discussions (PDF)

Video S1. In situ TEM movie shows the etching dynamics of Si nanopillars etched by 1% (w/v) aqueous KOH solution at 22 °C. As soon as etching of Si nanopillars begins, etch intermediates begin forming small nanoclusters on the surface of the nanopillars. Nanoclusters detach from the surface when they reach the size of 2−20 nm. At the end of the etching process, when the nanopillars are fully consumed, all of the nanoclusters are fully dissolved in the KOH solution (Figure 2A) (AVI)

Video S2. In situ TEM movie shows the etching dynamics of Si nanopillars etched by 4% (w/v) aqueous KOH solution at 22 °C. Similar to the 1% (w/v) KOH concentration, nanoclusters of etch intermediates form on the surface of the Si nanopillars during the etching (Figure 2B). Again, at the end of the etching process, nanoclusters are completely dissolved in the KOH solution (AVI)

Video S3. In situ TEM movie shows the etching dynamics of Si nanopillars etched by 5% (w/v) aqueous TMAH solution at 22 °C. In contrast to KOH etching, no formation of nanoclusters of etch intermediates is observed (Figure 4A) (AVI)

Video S4. In situ TEM movie shows the etching dynamics of Si nanopillars etched by 3% (w/v) aqueous KOH and 5% (w/v) TMAH solution mixture at 22 °C. Similar to TMAH etching, no formation of nanoclusters is observed (Figure 4B)(AVI)

Video S5. In situ TEM movie shows the etching dynamics of Si nanopillars etched by 3% (w/v) aqueous KOH and 1% (v/v) isopropyl alcohol solution mixture at 22 °C. Similar to TMAH etching, no formation of nanoclusters is observed (Figure 4C) (AVI)

■ AUTHOR INFORMATION

Corresponding Author

*E-mail: mirsaidov@nus.edu.sg.

ORCID

Petr Král: 0000-0003-2992-9027

Utkur Mirsaidov: 0000-0001-8673-466X

Notes

The authors declare no competing financial interest.

■ ACKNOWLEDGMENTS

This work was supported by the Singapore National Research Foundation's Competitive Research Program funding (NRF-CRP9-2011-04 and NRF-CRP16-2015-05) and the NUS Young Investigator Award (NUSYIA-FY14-P17) from the National University of Singapore. P.K. acknowledges support obtained from the NSF DMR #1506886 award. We thank Vasile Paraschiv, Guy Vereecke, and Harold Philipsen for their support and discussions.

■ REFERENCES

(1) Waldrop, M. M. *Nature* **2016**, *530*, 144−147.

(2) Kuhn, K. *IEEE Trans. Electron Devices* **2012**, *59*, 1813−1828.

(3) Thelander, C.; Agarwal, P.; Brongersma, S.; Eymery, J.; Feiner, L. F.; Forchel, A.; Scheffler, M.; Riess, W.; Ohlsson, B. J.; Gösele, U.; Samuelson, L. *Mater. Today* **2006**, *9*, 28−35.

(4) Goldberger, J.; Hochbaum, A. I.; Fan, R.; Yang, P. *Nano Lett.* **2006**, *6*, 973−977.

(5) Tomioka, K.; Yoshimura, M.; Fukui, T. *Nature* **2012**, *488*, 189−192.

(6) Kapadia, R.; Fan, Z.; Takei, K.; Javey, A. *Nano Energy* **2012**, *1*, 132−144.

(7) Huang, M. H.; Mao, S.; Feick, H.; Yan, H.; Wu, Y.; Kind, H.; Weber, E.; Russo, R.; Yang, P. *Science* **2001**, *292*, 1897−1899.

(8) Yan, R.; Gargas, D.; Yang, P. *Nat. Photonics* **2009**, *3*, 569−576.

(9) Craighead, H. G. *Science* **2000**, *290*, 1532−1535.

(10) Hannon, J. B.; Kodambaka, S.; Ross, F. M.; Tromp, R. M. *Nature* **2006**, *440*, 69−71.

(11) Panciera, F.; Chou, Y. C.; Reuter, M. C.; Zakharov, D.; Stach, E. A.; Hofmann, S.; Ross, F. M. *Nat. Mater.* **2015**, *14*, 820−825.

(12) Donnelly, V. M.; Kornblit, A. *J. Vac. Sci. Technol., A* **2013**, *31*, 050825.

(13) Choi, H.-J. *Semiconductor Nanostructures for Optoelectronic Devices*; Springer: Berlin, 2012.

(14) Shul, R. J.; Pearton, S. J. *Handbook of advanced plasma processing techniques*; Springer Science & Business Media, 2011.

(15) Pinion, C. W.; Christesen, J. D.; Cahoon, J. F. *J. Mater. Chem. C* **2016**, *4*, 3890−3897.

(16) Christesen, J. D.; Pinion, C. W.; Grumstrup, E. M.; Papanikolas, J. M.; Cahoon, J. F. *Nano Lett.* **2013**, *13*, 6281−6286.

(17) Choppin, G. R.; Pathak, P.; Thakur, P. *Main Group Met. Chem.* **2008**, *31*, 53−72.

(18) Nijdam, A. J.; Veenendaal, E. v.; Gardeniers, J. G. E.; Kentgens, A. P. M.; Nachtegaal, G. H.; Elwenspoek, M. *J. Electrochem. Soc.* **2000**, *147*, 2195−2198.

(19) Song-Sheng, T.; Reed, M. L.; Hongtao, H.; Boudreau, R. *J. Microelectromech. Syst.* **1996**, *5*, 66−72.

(20) Lee, J. W.; Jang, D.; Mouis, M.; Kim, G. T.; Chiarella, T.; Hoffmann, T.; Ghibaudo, G. *Solid-State Electron.* **2011**, *62*, 195−201.

(21) Wang, F.; Yip, S.; Han, N.; Fok, K.; Lin, H.; Hou, J. J.; Dong, G.; Hung, T.; Chan, K. S.; Ho, J. C. *Nanotechnology* **2013**, *24*, 375202.

(22) Zheng, H.; Smith, R. K.; Jun, Y.-w.; Kisielowski, C.; Dahmen, U.; Alivisatos, A. P. *Science* **2009**, *324*, 1309−1312.

(23) Ross, F. M. *Science* **2015**, *350*, 9886.

(24) Seidel, H.; Csepregi, L.; Heuberger, A.; Baumgärtel, H. *J. Electrochem. Soc.* **1990**, *137*, 3612−3626.

(25) Glembocki, O. J.; Palik, E. D.; Guel, G. R. d.; Kendall, D. L. *J. Electrochem. Soc.* **1991**, *138*, 1055−1063.

(26) Shikida, M.; Sato, K.; Tokoro, K.; Uchikawa, D. *Sens. Actuators, A* **2000**, *80*, 179−188.

(27) Palik, E. D.; Glembocki, O. J., Jr.; Burno, P. S.; Tenerz, L.; Heard, I. *J. Appl. Phys.* **1991**, *70*, 3291−3300.

(28) Allongue, P. *Phys. Rev. Lett.* **1996**, *77*, 1986−1989.

(29) Baum, T.; Schiffrin, D. J. *J. Electroanal. Chem.* **1997**, *436*, 239−244.

(30) Gosálvez, M. A.; Zubel, I.; Viinikka, E. Chapter 22 - Wet Etching of Silicon. In *Handbook of Silicon Based MEMS Materials and Technologies*, 2nd ed.; William Andrew Publishing: Boston, 2015; pp 470−502.

(31) Sander, R. *Atmos. Chem. Phys.* **2015**, *15*, 4399−4981.

DOI: 10.1021/acs.nanolett.7b00196
Nano Lett. 2017, 17, 2953−2958

(32) Preari, M.; Spinde, K.; Lazic, J.; Brunner, E.; Demadis, K. D. *J. Am. Chem. Soc.* **2014**, *136*, 4236−4244.
(33) Żegliński, J.; Piotrowski, G. P.; Piękoś, R. *J. Mol. Struct.* **2006**, *794*, 83−91.
(34) Michaud, P. T.; Babic, D. *J. Electrochem. Soc.* **1998**, *145*, 4040−4043.
(35) Palik, E. D.; Gray, H. F.; Klein, P. B. *J. Electrochem. Soc.* **1983**, *130*, 956−959.
(36) Gosálvez, M. A.; Sato, K.; Foster, A. S.; Nieminen, R. M.; Tanaka, H. *J. Micromech. Microeng.* **2007**, *17*, S1−S26.
(37) Bitzer, T.; Richardson, N. V.; Schiffrin, D. J. *Surf. Sci.* **1997**, *382*, L686−L689.
(38) Newton, T. A.; Huang, Y.-C.; Lepak, L. A.; Hines, M. A. *J. Chem. Phys.* **1999**, *111*, 9125−9128.

DOI: 10.1021/acs.nanolett.7b00196
Nano Lett. 2017, 17, 2953−2958